Supporting Information

Ramms et al. 10.1073/pnas.1313491110

SI Text

AFM Measurements. For atomic force microscopy (AFM) analyses, 12,000 keratinocytes were seeded on collagen I–coated (6 μg/cm^2 collagen, rat-tail; BD Bioscience) glass coverslips (Ø24 mm; Menzel-Gläser) 16–24 h before the experiment. AFM imaging of fixed and live cells was performed in contact mode using silicon tips (Nanosensor point probes-CONT-50) of nominal resonance frequency f_0 = 10–17 kHz and nominal spring constant k = 0.07–0.4 N/m. Images were processed using the JPK DP software. Indenters for probing cell elasticity were prepared by mounting silica microspheres of a nominal radius of 5 μm (G. Kisker GbR, PSI-5.0, surface plain) to silicon AFM tipless cantilevers of nominal resonance frequency f_0 = 7 kHz and nominal spring constant k = 0.04 N/m (Nanoworld Arrow TL1Au with Ti/Au back tip coating) using two-component glue (UHU plus Endfest 300; UHU). Smooth silica beads were picked under microscopy control. After attachment, microsphere diameters were measured using a confocal microscope equipped with an LD Plan Neofluar Ph.2 (40×/0.6) objective. AFM indentation curves were recorded at room temperature at sites of the nucleus and the cell body of single keratinocytes. Directly before measurements, cells on coverslips were washed once in PBS, mounted in the JPK Biocell chamber, and immersed in freshly prepared Hepes-buffered medium. Vitality of keratinocytes was checked visually. Before each experiment, the cantilevers were immersed in medium for 10 min to allow thermal equilibration and subsequent calibration using the thermal noise method. Measured spring constants ranged between 20 and 50 mN/m.

AFM Apparent Modulus Plots. A test to determine the optimal depth of indentation to be analyzed in AFM elasticity measurements consists of the analysis of the so-called "apparent-modulus" plots. For a material as heterogeneous and complex as a cell, Young's modulus E is not a constant value but varies according to the depth at which the AFM tip indents all of the different layers of soft biological material. Plateau regions in these $E(\delta)$ plots should be looked for, and the range of indentation δ giving rise to a roughly constant value of E should be used as a fit range during data analysis. By progressively extending the fit range (sphere model, AFM manufacturer's software) on single indentation curves, plateaus of E were identified between 200 and 600 nm (nucleus). No systematic plateau could be identified for measurements performed on the cell body. Fit ranges for further data analysis were chosen to be 500 and 200 nm for nucleus and cell body, respectively, also in light of the restrictions on the indentation depth imposed by the Hertz model ($\delta < 5-10\%$ of total sample thickness). Although different fit ranges impede the direct comparison of elasticity values for the cell body with those above the nucleus, analysis parameters were always kept identical between all analyzed cell lines.

Alternative Force-Distance Curve Analysis. Data fits using the Hertz model (Fig. S3 *A* and *B*) always yielded slightly curved residuals and contact points that were consistently and significantly below the measured curves. Therefore, this description is only a first approximation to the very complicated mechanical system and should be improved. Underlying reasons for the failure of this popular model are most likely roughness of cells (Fig. S4 *A* and *B*), sphere irregularities (Fig. S4*C*), and, most importantly, the nonhomogeneous and nonisotropic mechanical material properties of cells. We therefore developed an alternative approach by accurate determination of contact points from the approach curves alone (Fig. S5*A* and see below). Curves were then fitted using a standard power law function

$$F = A\delta^b. \qquad \textbf{[S1]}$$

In the following, we will call the prefactor A "apparent stiffness." If applicable, the exponent chosen is denoted by a subscript.

This approach can be connected to the Hertz model as follows. For indentations much smaller than the radius of the spherical indentor, which is in all our experiments, the solution of the Hertz model, Eq. **1**, can be simplified to yield

$$F(\delta) = \frac{4}{3}\frac{E}{(1-\nu^2)}\sqrt{R}\,\delta^{3/2}. \qquad \textbf{[S2]}$$

Thus, the Hertz model predicts a power law with exponent 3/2. The general power law function Eq. **S1** can be regarded as a generalization of the usual Hertz model.

Apparent stiffnesses $A_{3/2}$ resulting from such a model again proved WT cells to be significantly stiffer than keratin-deficient cells above the nucleus and cell body (Fig. S5 *B* and *C*; significance levels of 0.015 and 0.004, respectively).

In a next step, apparent stiffness A and exponent b were both selected as free fit parameters. From fitting all data curves we obtained Gaussian distributions of the exponent b with almost identical mean exponent values of 2.09 ± 0.75 (SD) for WT cells (n = 117) and 2.01 ± 0.65 for KtyI$^{-/-}$ cells (n = 109) (Fig. S5 *D* and *E*). The exponent was therefore fixed to a value of 2 and apparent stiffnesses A_2 were fitted for all force-distance curves. In contrast to the Hertz model the resulting fits showed minimal residuals without curvature and, most importantly, consistent contact points were used (Fig. S3*B*). The fit results also revealed a highly significant cell softening of ∼30% on keratin loss at nuclear and cell body positions (Fig. S3 *C* and *D*). The mean values were A_2 = 1,460 ± 1,060 N/m^2 (SD) (WT), A_2 = 1,120 ± 520 N/m^2 (KtyI$^{-/-}$, significance level 0.008) for the nucleus, and A_2 = 2,150 ± 1,400 N/m^2 (WT), A_2 = 1,610 ± 1,220 N/m^2 (KtyI$^{-/-}$, significance level 0.003) for the cell body.

On rescue cells, proper keratin network formation was assessed by fluorescence microscopy (Fig. 1*C*) before indentation in each of the analyzed cells (n = 46). The resulting force distance curves were also analyzed by the standard power law function (Eq. **S1**) with exponent b as a free parameter. Because K14 cells were also characterized by a mean value of 2.01 ± 0.75 (SD) (Fig. S5*E*), all curves were analyzed for apparent stiffness A_2 with b = 2 as before.

The Hertz model applies to the case of a smooth, spherical, and rigid indenter deforming a semiinfinite, perfectly elastic, and homogeneous substrate. To partially test these assumptions, surface roughness of the cells and of the spherical indenter were assessed. Reflection interference contrast microscopy (RICM) imaging of silica beads showed a variety of shape imperfections. Contact-mode AFM high-resolution live cell imaging performed on small portions of the plasma membrane's surface allowed to ascertain cell's roughness, which had average values of ∼50 nm as computed over an area of 500 × 500 nm^2 via

$$RMS_{rough} = \sqrt{\frac{1}{N}\sum_{i=1}^{N}(z_i - \bar{z})^2}, \qquad \textbf{[S3]}$$

where N is the image pixel number, z_i is the height at that pixel, and $\bar{z}$ is the average of z_i.

Indentation curves were analyzed by a Matlab-implemented software according to the following algorithms.

Raw data from force-distance approach curves were recalibrated by setting the sensitivity (nm/V) and spring constant (N/m) of the cantilever used for measuring, corrected for baseline offset and tilt and corrected for tip sample separation using the AFM manufacturer's data processing software. For differentiation, the curves (of typically ~20,000 data points) were averaged to yield 100 final data points.

The maximum position of the third derivative of the smoothed curve was used as the x coordinate of the contact point. The corresponding offset force value was calculated by averaging over a portion of the noncontact part of the unsmoothed curve (50 values next to the contact position).

The first 500/200 nm (nucleus/cell body, respectively) following the contact point of the recalibrated indentation curve were used as a fit range. The general power law $F(\delta) = A\delta^b$ (i.e., Eq. **S1**) was fitted via a least-squares method. A and b were the only free fit parameters. In a successive step of the analysis, b was user-constrained, thereby leaving the apparent stiffness A as the only free parameter. The residuals were computed as difference between measurement and best fit.

Magnetic Tweezers Measurements. For the magnetic tweezers, solenoids were fabricated with a VACOFLUCX 17 (VACUUMSCHMELZE GmbH & Co.) core (2.28 mm in diameter), which has a saturation magnetization of 2.2 T. An electrochemical etching process described by ref. 1 was applied to produce tips with a radius of 5 μm. Initially a 10-mm section of one side of the core was mechanically reduced to a diameter of ~1 mm (Fig. S7*A*). This section of the core was exposed to the etching solution, which is comprised of 80 mL 85% (vol/vol) phosphoric acid, 70 mL 95.0–97.0% (vol/vol) sulfuric acid, and 50 mL distilled water, whereas the rest of the core was protected by a photoresist (AZ 4562; MicroChemicals GmbH) (Fig. S7*B*). A DC voltage of 12 V was applied (Fig. S7*C*). The lower part of the shield was removed after the core section exposed to the solution was etched to 40% of the original diameter. Etching was continued with a reduced voltage of 8 V (Fig. S7*D*). The etching was stopped when the distal part of the core dropped down (Fig. S7 *E* and *F*). The coil surrounding the magnetic core was produced from 100-μm copper wire (3,000 turns). For cooling, the isolated coil was housed in a surrounding chamber, which was circulated by cold water.

1. Matthews BD, LaVan DA, Overby DR, Karavitis J, Ingber DE (2004) Electromagnetic needles with submicron pole tip radii for nanomanipulation of biomolecules and living cells. *Appl Phys Lett* 85(14):2968–2970.

To calibrate the particle movement, Stokes' law was used. The magnetic force applied to a bead of radius r moving with velocity v in a fluid of known viscosity η can be calculated via Stokes' law

$$F = 6\pi r v. \quad \textbf{[S4]}$$

Dynabeads M-270 with a diameter of 2.8 μm and an SD of 1.4% were used for force calibration experiments. The beads were immersed in three different fluids with viscosities of 1,000, 3,500, and 5,000 centiStokes (vinyl terminated polyDimethylsiloxanes; abcr GmbH & Co.). The current supply of the tweezers coil was kept to 215 mA, both for calibration and further measurements. The beads and the tip of the magnetic tweezers were simultaneously tracked to determine both the velocity and the distance between bead and tip.

Fig. S8*A* shows the force-distance dependence of three magnetic beads, each deflected in one of the three above described calibration solutions. The movements of the beads were within an angle of 5° with respect to the tweezers axis. The fitting curve

$$F(x) = a(x + c)^b, \quad \textbf{[S5]}$$

where x denotes the bead-core-distance. Parameters a, b, and c were determined by fitting Eq. **S5** to the measured force distance relation displayed in Fig. S8*A*. The result was used for calculating forces acting in magnetic tweezers experiments on cells.

For magnetic tweezers experiments, cells were grown to confluency on collagen-coated glass slides (35 mm Ø); 250 mg of superparamagnetic M-270 Dynabeads (Invitrogen) was "shot" onto the cells using a PDS-1000/He particle delivery system (BioRad). Beads remaining outside the cells were removed by rigorous washing. After trypsination and reseeding, single cells with single incorporated beads were selected for analyses after 12 h. An Eppendorf micromanipulator 5171 (Eppendorf) was used to place the tip of the tweezers next to the cell at bead height and at a lateral distance of 40–60 μm. Repeated rectangular pulses of 5 s in length were applied every 10 s and recorded at a frequency of 50 frames/s using an EOS 650D/Rebel T4i single-lens reflex (SLR) camera (Canon). Beads still attached to the outside of the cells had only loose contact and were removed by the first pulse. The entire setup was placed in a climate chamber heated to 37 °C. The bead and magnetic tweezers tip position were tracked over time using implemented algorithms of Adobe After Effect CS4 (Adobe Systems) and Fiji.

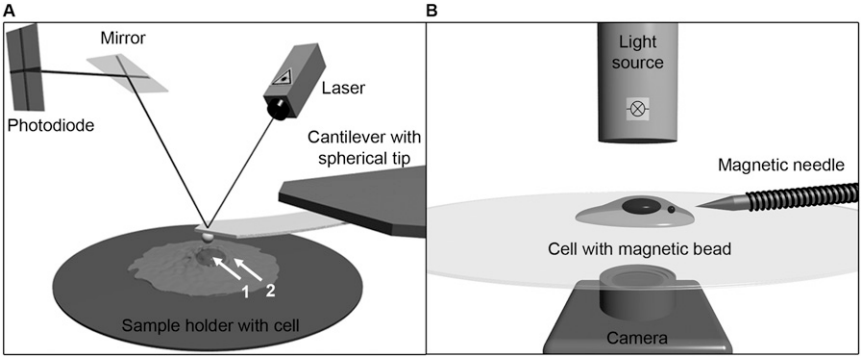

Fig. S1. (*A*) Scheme of the AFM setup used for single cell elasticity measurements. A tipless cantilever with a silica bead attached indents cells at nucleus (*1*) and cell body (*2*). (*B*) Diagram of the magnetic tweezers setup. A superparamagnetic bead transferred into the cell's cytoplasm is subjected to periodic magnetic pulses produced by the needle-shaped core of an electromagnet.

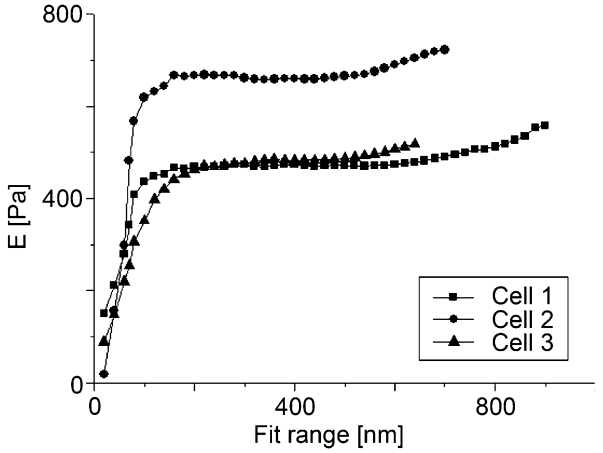

Fig. S2. Examples of the dependency of the Young's modulus *E* on the portion of indentation curve taken as fit range. For measurements performed on the nucleus a plateau is observable between 200–600 nm.

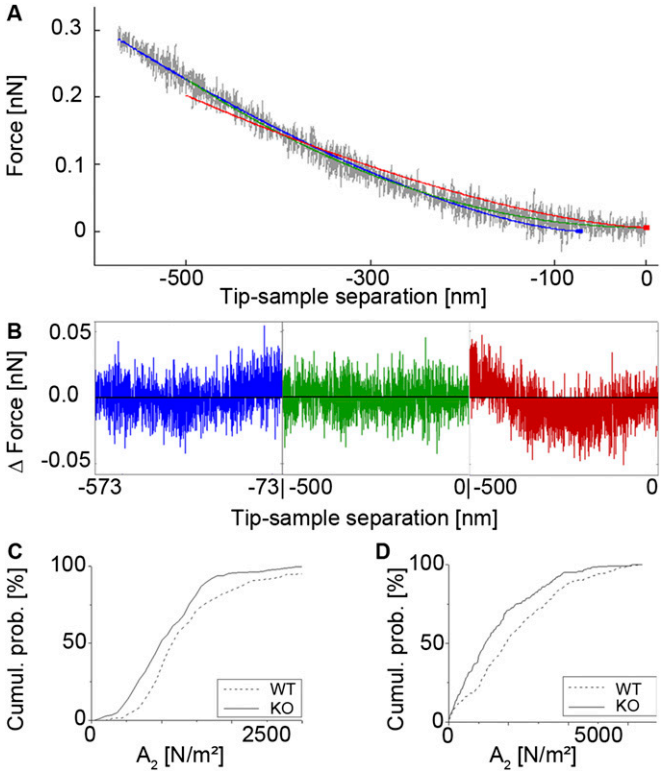

Fig. S3. Fit residuals and apparent stiffness *A* of WT and KtyI$^{-/-}$ cells. (*A*) Fitted portion (500 nm) of a force-distance curve recorded on a nucleus. Gray, data; blue, AFM manufacturer's software fit (Eq. **2**, sphere model); blue dot, fitted contact point; green, fit of a power law (Eq. **S1**) with fixed exponent $b = 2$; red, same fit with $b = 1.5$ (Hertz model, cf. Eq. **S2**); red dot, contact point determined directly from measured curve as described in *SI Text*. (*B*) Corresponding fit residuals. (*C*) Cumulative histograms of the apparent stiffness A obtained from fitting the power law function $F(\delta) = A\delta^b$ with $b = 2$ to the approaching portion of all force-spectroscopy curves recorded on nucleus (fit range: 500 nm, $n_{WT} = 89$, $n_{KO} = 110$) and (*D*) cell body (fit range: 200 nm, $n_{WT} = 117$, $n_{KO} = 113$).

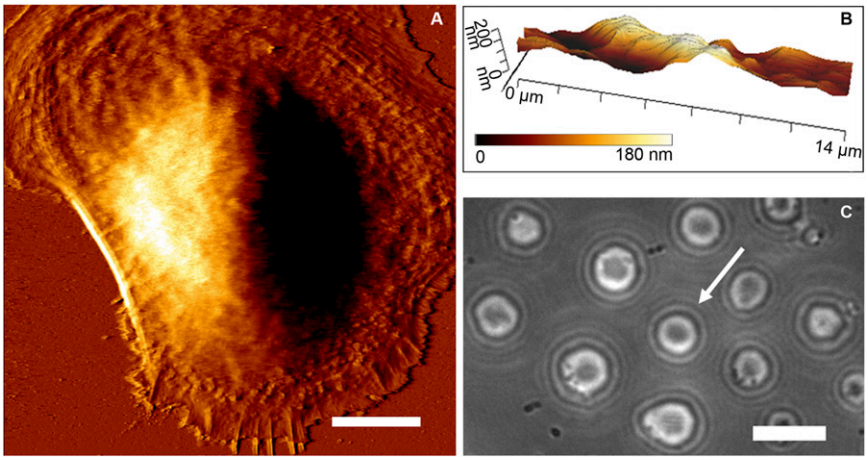

Fig. S4. (*A*) Contact-mode AFM error signal image of a live WT keratinocyte. (Scale bar, 10 µm.) (*B*) 3D reconstruction of the surface topography of a 14 × 1.3-µm^2 portion of the plasma membrane used to estimate surface roughness. (*C*) Reflection interference contrast microscopy (RICM) image showing shape and surface roughness of the silica beads used for AFM cantilever modification. The arrow marks a representative bead selected for mounting. (Scale bar, 10 µm.)

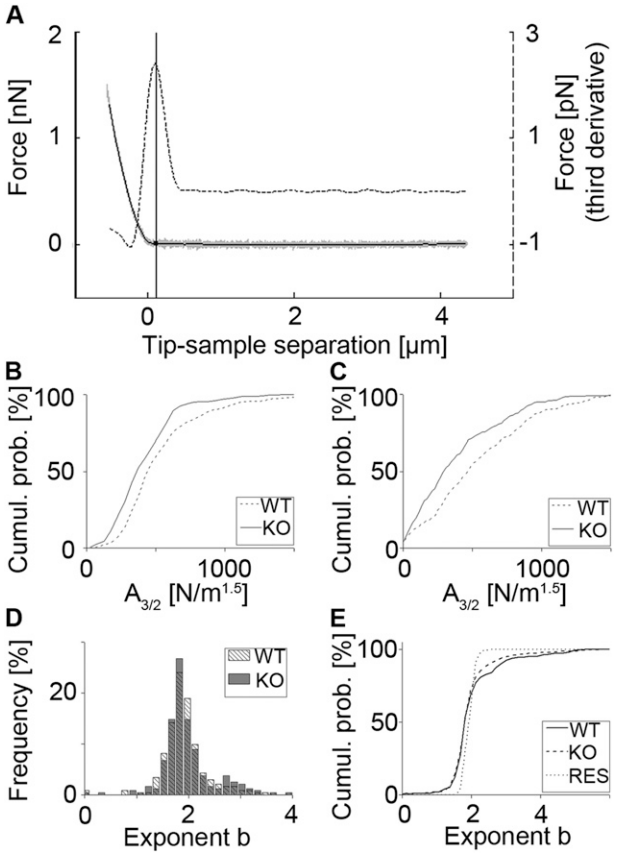

Fig. S5. (*A*) Plot showing contact point identification on a typical AFM indentation curve recorded on a cell's nucleus. Gray, original data; dark gray, smoothed data used for third derivative calculation (dashed line). The contact point is identified as the maximum of the curve's third derivative. Zero of tip-sample separation axis: contact point as identified by the AFM manufacturer's data analysis software. (*B*) Cumulative histograms of the apparent stiffness *A* obtained from fitting the power law function $F(\delta) = A\delta^b$ with an exponent $b = 1.5$ (Hertz model) to force-indentation curves recorded on WT/KtyI$^{-/-}$ (KO) nucleus (n_{WT} = 89, n_{KO} = 110, different on a significance level of 0.015) and (*C*) cell body (n_{WT} = 117, n_{KO} = 113, different on a significance level of 0.004). (*D*) Frequency histogram of the exponent *b* obtained from fitting the power law function to the extended portion of all indentation curves recorded on nucleus (fit range: 500 nm) and cell body (fit range: 200 nm) of WT (n = 118) and KO (n = 116) cells. (*E*) Corresponding cumulative histogram, showing the almost perfect overlap of the distributions (data recorded on RES cells are included). A total of four cantilevers were used during the complete series of experiments.

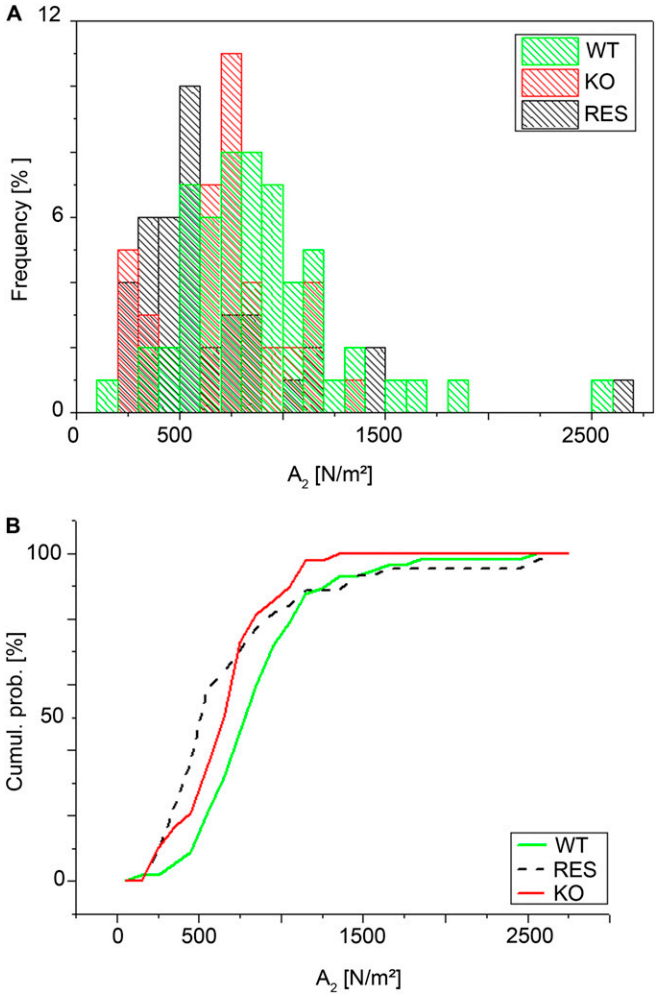

Fig. S6. (*A*) Histogram showing the distribution of apparent stiffness A_2 obtained from indentation experiments performed on the nucleus of WT ($n = 57$), Ktyl$^{-/-}$ (KO; $n = 51$), and rescue (RES; $n = 46$) cells and (*B*) corresponding cumulative histograms.

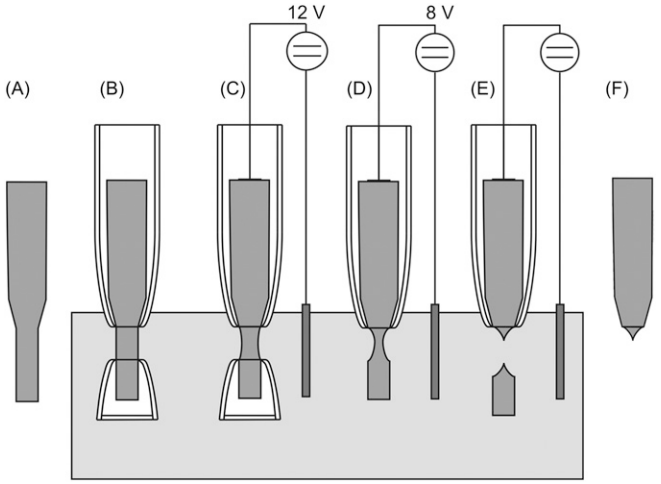

Fig. S7. Electrochemical etching process outline. (*A*) A lathed core before etching. (*B*) Two fitted pipette tips were mounted onto the core surface. The lower one had to be sealed to protect the end of the core. The length of the tip was controlled by the exposed length of the core. (*C*) A 12-V DC voltage was applied on the core to etch the exposed part electrochemically. (*D*) Once the core diameter is etched down to 40% of the original, the lower shield was removed. The voltage was set to 8 V to avoid too large etching currents. (*E*) The power switched off once the distal part dropped down. (*F*) The upper shield was removed.

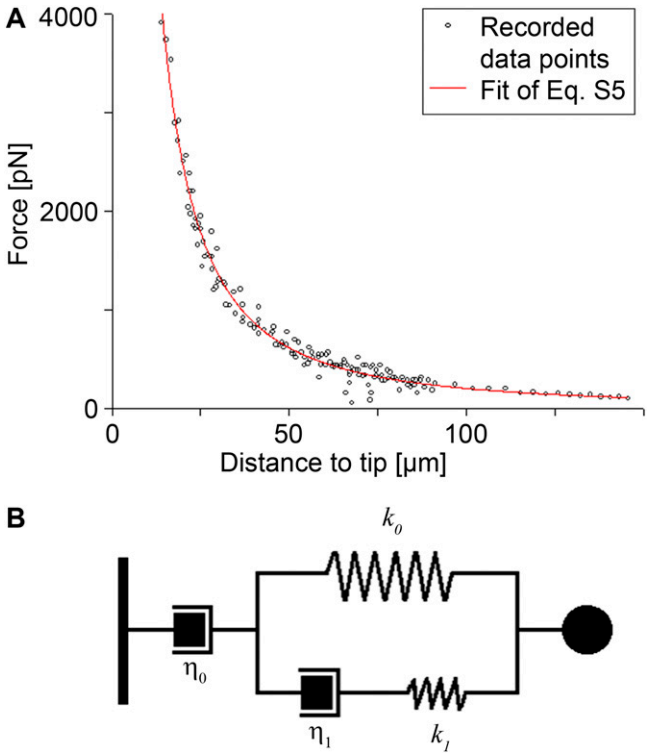

Fig. S8. (*A*) Magnetic tweezers force-distance calibration curve. (*B*) Schematics of the mechanical equivalent circuit used for fitting the viscoelastic response of the cytoplasm-incorporated magnetic beads used in magnetic tweezers experiments (1). In Eq. **2**, we used the relaxation time τ that is related via $\tau = \frac{\gamma_1(k_0+k_1)}{k_0 k_1}$ according to ref. 2 with the parameters of the equivalent circuit shown here.

1. Matthews BD, LaVan DA, Overby DR, Karavitis J, Ingber DE (2004) Electromagnetic needles with submicron pole tip radii for nanomanipulation of biomolecules and living cells. *Appl Phys Lett* 85(14):2968–2970.
2. Bausch AR, Ziemann F, Boulbitch AA, Jacobson K, Sackmann E (1998) Local measurements of viscoelastic parameters of adherent cell surfaces by magnetic bead microrheometry. *Biophys J* 75(4):2038–2049.